Characteristics of calcium carbonate fouling on heat transfer surfaces under the action of electric fields

Xu, Zhiming; Chang, Hongliang; Wang, Bingbing; Wang, Jingtao; Zhao, Qi

Published in:
Journal of Mechanical Science and Technology

DOI:
10.1007/s12206-018-0648-0

Publication date:
2018

Document Version
Peer reviewed version

Characteristics of Calcium Carbonate Fouling on Heat Transfer Surface under the Action of Electric Fields

Zhiming Xu[1], Hongliang Chang[1*], Bingbing Wang[1], Jingtao Wang[1] and Qi Zhao[2*]

[1] *School of Energy and Power Engineering, Northeast Electric Power University, Jilin 132012, China*
[2] *School of Science and Engineering, University of Dundee, Dundee DD1 4HN, U.K.*

Abstract

The present study conducted the effect of electric fields in calcium carbonate ($CaCO_3$) scale formation on heat transfer surface. The electric fields ranging from 0 to 4000 V on fouling properties of $CaCO_3$ were investigated. The results revealed that the optimal electric voltage lied at around 500 V, at which the asymptotic value of fouling resistance and deposited weight were minimal, corresponding to respectively 52.8 % and 61.3 % reductions when compared to results recorded at 0 V. At higher voltages of 3000 or 4000 V, the asymptotic value of fouling resistances and weight of fouling deposits increased relative to those obtained at 0 V. At 0 V, the SEM images of fouling deposits showed mainly aragonites with sharp and needle-like crystal structures. As the applied voltage rose, the structure of $CaCO_3$ fouling changed from aragonites to spherical vaterites.

Keywords: fouling characteristics; electric field; anti-fouling; $CaCO_3$ fouling

1. Introduction

Calcium carbonate ($CaCO_3$) is one of the most common fouling found on heating surfaces of cooling-water systems [1-5]. The $CaCO_3$ fouling on the heat transfer surfaces significantly decreases the thermal efficiency of heat exchanges since fouling deposits have very low thermal conductivities. The continuous deposition of fouling on heating surfaces would also lead to the reductions in flow-area, hence requiring more pumping power to maintain the flow. The cost of cleaning and reduced output can extremely be high for heavily fouled heat exchangers.

The most utilized methods for controlling fouling are based on chemical method and physical methods. The chemical method is carried out by adding fouling-inhibiting chemicals to effectively mitigate the mineral fouling. These include chelation [6], dispersion [7] and inhibition [8], The chemical based methods are simpler with high feasibility. However, they are relatively expensive and could substantially change the

* Corresponding author. Tel:+86 13844244549. Email address { HYPERLINK "mailto:Changhongliang1112@yeah.net" } (HL Chang); { HYPERLINK "mailto:q.zhao@dundee.ac.uk" } (Q. Zhao)

water chemistry [9]. The physical methods are mainly performed by means of various devices to reduce mineral fouling. These include permanent magnets [10-12], electromagnets [13-19], and electrodes [6, 20, 21, 24]. Water magnetic and electromagnetic based treatments have been investigated for decades, and results showed that the water purity increased and fouling formation reduced after the passage of magnetic or electromagnetic field through the water. Calcium carbonate fouling involves the formation of calcite, vaterite, and aragonite. Some studies reported that the structure of $CaCO_3$ fouling changed and aragonite deposition increased as magnetic or electromagnetic fields are applied [14].

Recently, in addition to magnetic and electromagnetic treatments, the electric field generated between two electrodes has also been used to mitigate $CaCO_3$ fouling. For instance, Tijing et al [9] investigated the anti-fouling performance of heating copper tube surfaces by radio frequency electric fields. They used electric fields with three different voltages and two frequencies and artificial hard water for fouling formation. They found that the applied electric field reduced $CaCO_3$ fouling. The $CaCO_3$ fouling exhibited blunt crystal structures upon application of the electric field, while $CaCO_3$ fouling exhibited different sharp and pointed structures in absence of electric fields. Tijing et al [21] further examined the impact of high-frequency electric fields on water chemistry, deposition composition, and fouling resistance. They demonstrated that calcium contents of fouling deposits dropped by 4-49 %, and asymptotic fouling resistances decreased by 88 % at high-frequency electric fields. Clearly, the use of high-frequency electric fields showed elevated anti-fouling efficiencies with low power consumptions due to the absence of formed of closed circuits using two electrodes.

Therefore, electric fields could be adopted to mitigate mineral fouling on heat transfer surfaces in industrial applications. To the best of our knowledge, no reports dealing with optimum electric voltages minimizing fouling were so far published. In the study, to better understand the relationship between applied voltages and mineral fouling characteristics, $CaCO_3$ fouling subjected to direct current (DC) electric fields ranging from 0 to 4000 V were performed for the first time. The influence of electric fields on formed fouling and structures of $CaCO_3$ fouling were investigated and the results were discussed.

2. Materials and methods

2.1 Experimental setup

Fig. 1 shows the schematic diagram of the experimental setup used in this study, It mainly consisted of a thermostatic water tank, agitator for mixing testing solutions, electromagnetic flow meter, DC power supply, high voltage supply, and computer controlled data acquisition system. The working fluid would enter the loop from the water tank through the isolated pipes, and then continuously circulate thanks to the centrifugal pump. An electromagnetic flow meter was installed at the trajectory line of the fluid to measure the flow rate with least uncertainties. The temperatures of the inlet and outlet

fluids were measured by two PT-100 resistance thermometers located just before and after the testing unit. The two electrodes were oriented in parallel to each other at the distance of 40 mm.

{ EMBED Visio.Drawing.11 * MERGEFORMAT **}**

Fig.1. The schematic diagram of the experimental setup

Fig. 2 depicts a three-dimensional sketch of the testing unit, consisting of 316a stainless steel sleeve and Lucite tube. The 316a stainless steel sleeve was made of an electrically heated cylindrical rod and four PT100 resistance thermometers. The length of the stainless steel sleeve measured 420 mm, and that of the heating section was 150 mm (100 mm starting from the rod). The steel sleeve was concentrically located within a surrounding vertical Lucite tube. The electrically heating rod (diameter 14 mm, length 250 mm) was placed in the center of the stainless steel sleeve. To minimize the thermal contact resistance, high-quality heat conducting oil (the Star Heat Transfer Paste) was injected into the sleeves. The test heater was connected to a DC power supply allowing changes in heat flux between 0 and 255 $kW \cdot m^{-2}$. Due to insulation of both ends of the heating rod, the axial heat transfer of the electrically heating rod could be ignored. The wall temperature of the test section was measured by four PT100 resistance thermometers with diameter of 2 mm and length of 175 mm.

The working fluid flowed through the annulus in upward direction between the stainless steel sleeve and Lucite tube, and the effect of gravity on the fouling process might be ignored. The equivalent diameter of the annular experimental channel was 20 mm. The working fluid will flow back to the water pipe after experiments to form close loops. The external electric field was supplied by a high voltage generator composed of high-voltage power supply and two parallel electrode plates. The high voltage power supply could deliver an output voltage ranging from 0 to 30 kV, maximum output current of 1 mA, and load regulation accuracy of less than or equal to 0.1 %. The parallel electrode plates were made of copper with sizes of 360 mm×30 mm×1 mm. The test heater and applied electric field belong to two isolated systems respectively. The test heater was connected directly to a DC power (GD-120V 20A), while the external electric field was provided by the high voltage power (DW-P303-1ACFO). The high voltage power supply was not used for the test heater, so it was directly connected to the parallel electrode plates. All measured parameters, including pressure, temperature and volume flow were collected and stored in data acquisition system for further analysis

{ EMBED Visio.Drawing.11 * MERGEFORMAT **}**

Fig.2. Schematic diagram of the experimental test unit.

2.2. Preparation of test solutions and experimental methods

The artificial hard water was prepared by mixing appropriate amounts of sodium bicarbonate ($NaHCO_3$) and calcium chloride ($CaCl_2$) powders. Calcium carbonate was formed by the reaction of $NaHCO_3$ with $CaCl_2$ according to Eq. (1):

$$CaCl_2 + 2NaHCO_3 \rightarrow CaCO_3 + 2NaCl_2 + H_2O + CO_2 \quad (1)$$

$NaHCO_3$ (25.20 g) and $CaCl_2$ (16.65 g) at molar the ratio of 2:1 were dissolved in two separate beakers containing 100 ml distilled water. Prior to experiments, the surface of testing unit, thermostatic water tank, electromagnetic flow meter and pipes were all washed with diluted hydrochloric acid solution to remove fouling. Afterward, distilled water (30 L) was added to the water tank, and an electric field was applied then left for 15 hours until stabilization of the system. The inlet temperature of the solution was controlled at 40 ℃, the initial average temperature of the heated surface at clean conditions was set to 75±0.3 ℃， and the volume flow rate was 0.75±0.005 $m^3\ h^{-1}$. The flow was adjusted manually and the difference in volume flow rates in each tests was set to about 0.05 $m^3\ h^{-1}$. The Reynolds number based on bulk velocity and hydraulic diameter was recorded at about 10000 and fluid was categorized as turbulent flow. The salt solution was slowly added to the water tank at motorized stirring of 250 rpm to ensure uniform mixing. The initial hardness of the working fluid was measured as 500±20 ppm (or $mg \cdot L^{-1}$). After addition of salt solution, the liquid properties instantaneously changed , leading to transient fluctuations in the experimental data. Therefore, the experiment after six minutes was set as the starting point.

2.3. Fouling resistance

The overall fouling resistance was calculated from the total heat transfer coefficient at clean and fouled conditions. The fouling resistance R_f ($m^2 \cdot K\ W^{-1}$) was defined by Eq. (2).

$$R_f = \frac{1}{k} - \frac{1}{k_0} \quad (2)$$

where k_0 and k denote to the overall heat transfer coefficients at clean and fouling conditions, respectively.

The total heat transfer coefficient k ($W\ K^{-1}\ m^{-2}$) was calculated by Eq. (3).

$$k = \frac{q}{T_{wm} - T_b} \quad (3)$$

The above formula was based on approximate cylinder heat conduction equation with less error in the present study. The heat flux of the heating surface q ($W\ m^{-2}$) was calculated by heating rod power Q (W) and area of the heated surface A (m^2) according to Eq. (4).

$$q=\frac{Q}{A}=\frac{Q}{\pi dl} \tag{4}$$

The local bulk temperature T_b (℃) was considered as the arithmetic average value of the inlet and the outlet temperatures of the fluid:

$$T_b=\frac{1}{2}\left(T_{in}+T_{out}\right) \tag{5}$$

where T_{wm} (℃) represents the arithmetic average of the surface temperature for all four PT100 resistance thermometers, T_{in} (℃) is the inlet temperature of the fluid, and T_{out} (℃) is the outlet temperature of the fluid.

2.4. Experimental uncertainties

The uncertainties in the experimental results were analysed by the procedures proposed by Zhang [22]. The error would mainly be induced by the direct measurement and data transmission. The root mean square value and error analysis can be calculated by Eq. (6).

$$\partial k=\sqrt{\sum_{i=1}^{n}\left(\frac{\partial k}{\partial X_i}\delta X_i\right)^2} \tag{6}$$

{ EMBED Equation.DSMT4 * MERGEFORMAT } is the measurement error of experimental setup and represents the error transfer coefficient.

The relative error of fouling resistance ε can be expressed as by Eqs. (7-9).

$$\varepsilon=\frac{\delta R_f}{R_f} \tag{7}$$

$$\delta R_f=\pm\sqrt{\left(\frac{\partial R_f}{\partial k}\delta k\right)^2+\left(\frac{\partial R_f}{\partial k_0}\delta k_0\right)^2} \tag{8}$$

$$\frac{\partial R_f}{\partial k}=-\frac{1}{k^2} \qquad \frac{\partial R_f}{\partial k_0}=-\frac{1}{k_0^2} \tag{9}$$

Considering the above error analyses, the obtained error of heat transfer coefficient was around 0.57 % based on Table 1.

Table 1. Summary of the uncertainty analysis

Parameter	**Uncertainty**
Measuring wire resistance	±0.05 %
Temperature (℃)	±0.23 %

Water flow rate (lit.min^{-1})	±0.5 % of readings
Voltage (V)	±0.1 % of readings
Current (A)	±0.1 % of readings
Flow heat transfer coefficient (W m^{-2}·K^{-1})	±0.57 %

The maximum relative error of fouling resistance ε was estimated to 5.03 % in the present study, and the measured errors of parameters were less than 1 %.

3. Results and discussions

3.1. Repeatability of experiment data

To verify the repeatability of the experiments, tests at the same initial conditions consisting of no-treatment and applied 0 V and 500 V were conducted. The inlet temperature was 40 ℃ and the initial temperature of the hot stainless steel surface was 75±0.3 ℃. The initial water hardness and volume flow rate were 500±20 ppm (mgL^{-1}) and 0.75±0.005 m^3 h^{-1}, respectively. Figure 3 shows the change in fouling resistances at the electric voltages of 0 V and 500 V. It can be seen that the fouling resistance curves for the experiments performed at the same initial conditions (0 V or 500V) almost overlapped, indicating a setup with good repeatability and stability. The maximum difference in the asymptotic value of fouling resistance was estimated to 2.01 % for 0 V and 2.18 % for 500 V. This difference originated from the small differences in the initial temperature of heated surface and volume flow rate of the fluid. Therefore, each test was repeated twice and the average values of fouling resistances at the same operating conditions were calculated. Figure 3 also illustrated that the asymptotic value of fouling resistance was remarkably lower at 500 V compared to that obtained at 0 V, suggesting that the electric voltage had a significant influence on fouling resistance.

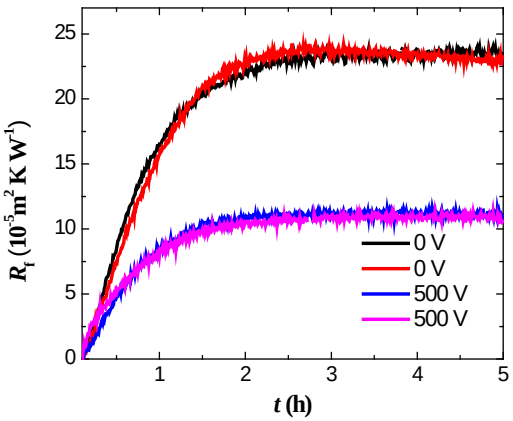

Fig. 3. Repeatability of the experimental data

3.2. Effect of electric voltage on fouling resistance

A series of experiments were designed and validated to vertify the effects of electric voltages on fouling characteristics. Electric voltages of 0 V, 20 V, 60 V, 100 V, 500 V, 1000 V, 3000 V and 4000 V were tested on the setup at the same conditions described in Section 3.1. The results of fouling resistance at these applied electric fields are shown in Fig.4, and the corresponding asymptotic values are displayed in Fig.5.

No apparent induction period was observed due to the extremely high water hardness and wall temperature of the system tested with or without the electric fields (Figure 4), consistent with date reported by Tijing et al [21]. At 0 V, the $CaCO_3$ fouling increased rapidly during the first stages then reached an asymptotic value of 23.5×10^{-5} m^2 K W^{-1} after 2.5 h. At 20 V, the fouling resistance curve appeared similar to that obtained at 0 V, indicating no significant difference in fouling formation at lower electric field. As the electric voltage rose (60 V, 100 V, 500 V), the asymptotic values of fouling resistances decreased. At 500V, the asymptotic value of fouling resistance reached the lowest value of 11.1×10^{-5} m^2.K W^{-1}. Afterward, the asymptotic values of fouling resistance increased as the electric voltage further rose (1000 V, 3000 V, 4000 V). Obviously, an optimal electric voltage of 500 V existed, where the asymptotic value of fouling resistance was minimal. The experiments suggested that when voltages continuously increased to 3000 V or 4000 V, fouling formation was accelerated, and the asymptotic value of fouling resistance was larger than that obtained at 0 V. Thus, it could be concluded that electric field could also promote fouling formation at voltages above the threshold value.

The effects of electric fields on asymptotic values of fouling resistances are given in Fig. 5. The asymptotic value of fouling resistance first decreased then increased as voltage rose. A minimum value of asymptotic fouling resistance was recorded as (11.1×10^{-5} m^2·K W^{-1}) at 500 V. This reduced the fouling resistance by 52.8 % when compared to that obtained at 0 V. The largest asymptotic value of fouling resistance was obtained at 4000 V (40.80×10^{-5} m^2·K W^{-1}), increasing the fouling resistance by 73.7 % when compared to that at 0 V.

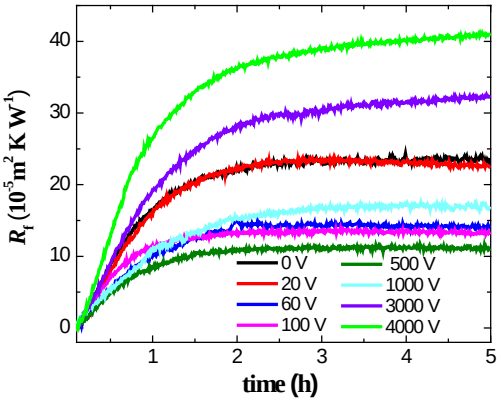

Fig. 4. Fouling resistance as a function of time at various applied electric fields

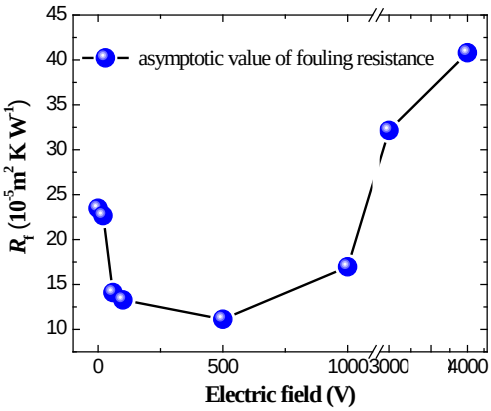

Fig. 5. Asymptotic values of fouling resistance at various applied electric fields.

3.3. Effect of electric voltage on the weights of fouling deposits

A weighting method was used to analyze the masses of the fouling deposits. Stainless steel coupons with sizes of 30 mm×10 mm×2 mm were prepared and fixed on the heating surface. The test coupons were weighed before and after the experiment [23]. The mass of the fouling film deposited on the coupon *W*s can be estimated using Eq. (10).

{ EMBED Equation.DSMT4 * MERGEFORMAT } （10）

where W_f is the weight of the fouled coupon in mg and W_0 is the weight of the initial coupon in mg.

Figure 6 shows the weight of the fouling deposits at various applied electric fields. As voltage increased, the weight of fouling deposits decreased until 500 V then rose after that. At 0 V, the weight of fouling deposit was estimated to 6.2 mg while at 500 V, the mass reduced to a minimum of 2.4 mg, This was equivalent to a 61.3 % reduction relative to that obtained at 0 V. When the electric field increased to 3000 V and 4000 V, the weights

of the fouling deposits reached 8.5 mg and 10.1 mg, respectively. These values corresponded to respectively 37.1% and 62.9 % increase relative to that obtained at 0 V. These results further demonstrated that strong electric fields promoted formation of $CaCO_3$ fouling on the heating surface.

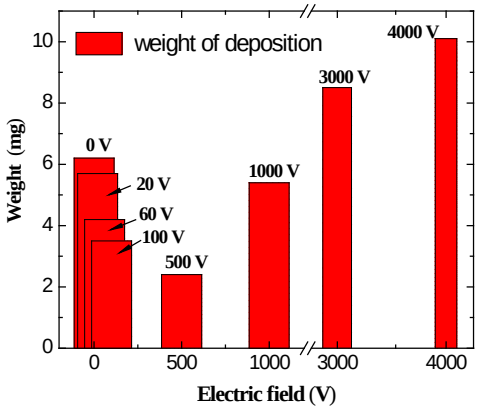

Fig. 6. The weight of fouling deposits as a function of the applied electric fields

In general, electric fields could have two effects on $CaCO_3$ solution: increasing the dissolved ions to collide more frequently and promoting $CaCO_3$ salts in ionized solutions to release Ca^{2+} and CO_3^{2-} ions. The possible mechanism dealing with the effect of electric field on the fouling characteristics may be summarized follows: During applied voltages, the collisions between Ca^{2+} and CO_3^{2-} ions in solution occurs. Due to the existence of electric field force, the ions with different charges move in the direction under the action of electric field, thus increasing the frequency of ion collisions. As a result crystallization becomes more frequently. Therefore, more crystallization would occur in solutions before being flowed into the experimental test unit under the applied electric field, the formation of fouling on the heating surface could be mitigated or at least inhibited [9]. At voltage rose, the dissolved ions will be crystallized, reducing fouling. When the applied voltage exceeds the threshold value (500 V), the second effect started to play a more important role than the first. The extent of $CaCO_3$ ionization became superior to crystallization. The higher voltage, the stronger ionization effect of calcium carbonate($CaCO_3$). The concentration of Ca^{2+} and CO_3^{2-} ions in solution increased and then larger numbers of Ca^{2+} and CO_3^{2-} ions crystallized on the heating surface. Therefore, an optimal voltage would exist, where fouling formation was minimal.

3.4. SEM analysis of fouling deposits

To analyze the effect of the electric field on structure of $CaCO_3$ fouling deposits, scanning electron microscope (SEM) was used to analyze the fouling structures. SEM images of $CaCO_3$ crystal structures without and with electric fields are exhibited in Fig. 7. The $CaCO_3$ crystal structures appeared very different at various applied electric field intensities. At 0 V (Fig. 7a), the fouling deposit was composed of mainly aragonites with

sharp and pointed needle-like crystal structures. The aragonites were located at bottom of the fouling layer and small amounts of vaterites with spherical structures in upper layer.

At 500 V (Fig. 7b), the sizes of both aragonites and spherical vaterites became smaller than those observed at 0 V, and distribution of the aragonites and the vaterites was scattered. When voltage increased to 3000 V, the amounts of sharp and needle-like aragonites became fewer (Fig. 7c), and $CaCO_3$ fouling deposit was composed of mainly spherical vaterites. Furthermore, the distribution of the spherical vaterites became denser when compared to the morphology observed at 500 V. In summary, the $CaCO_3$ fouling structure changed from aragonites to vaterites as the applied electric voltage increased.

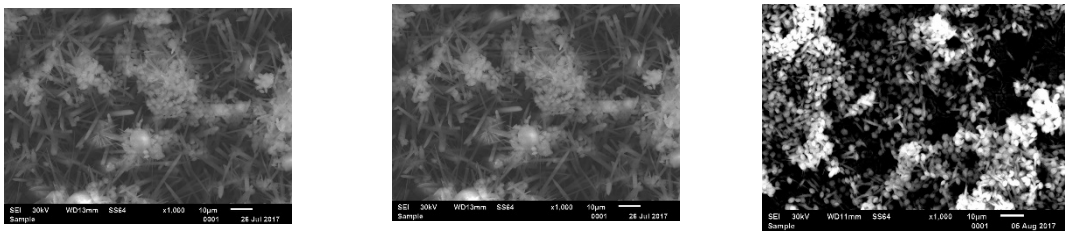

(a) 0 V (b) 500 V (c) 3000 V

Fig. 7. SEM images of fouling deposits for the electric voltages of at 0 V, 500 V, and 3000 V.

4. Conclusions

The effects of electric fields on $CaCO_3$ fouling properties were investigated. The electric field was generated by two copper electrodes at strengths of 0 V, 20 V, 60 V, 100 V, 500 V, 1000 V, 3000 V, and 4000 V. As voltage rose from 0 V to 500 V, both fouling resistances and deposited weights decreased until 500 V, then increased from 500 V to 4000 V. The optimum anti-fouling voltage was indentified as 500 V, which reduced the asymptotic value of fouling resistance and weight of fouling deposit by respectively 52.8 %, and 61.3 % when compared to values obtained at 0 V. The increase in the applied voltage to 3000 V or 4000 V induced larger asymptotic values of fouling resistances and weights of fouling deposits on the test coupon when compared to those recorded at 0 V. The SEM images of fouling deposits showed mainly aragonites with sharp and needle-like crystal structures at 0 V. As the applied voltage rose, the structure of $CaCO_3$ fouling changed from aragonites to spherical vaterites.

Acknowledgement

This work was supported by the National Natural Science Foundation of China (Grant numbers 51476025, 51706038).

Nomenclature

A	:area of heated surface
d	:diameter of stainless steel sleeve
k	:overall heat transfer coefficients at fo uling conditions
k_0	:overall heat transfer coefficients at cle an conditions
l	:length of heating section
Q	:heating rod power
q	:heat flux of heating surface
R_f	:fouling resistance
T_{wm}	:arithmetic average of surface tempera ture
T_b	:arithmetic average value of inlet and o utlet temperature of the fluid
T_{in}	:inlet temperature of fluid
T_{out}	:outlet temperature of fluid
W_s	:weight of fouling deposit on the coup on
W_f	:weight of fouled coupon
W_0	:weight of initial coupon
e	:relative error of fouling resistance

References

[1] Y.I. Cho, A.F. Fridman, S.H. Lee, W.T. Kim, Physical water treatment for fouling prevention in heat exchangers, Adv. Heat Transfer. 38 (2004) 1-72.

[2] J. Macadam, S.A. Parsons, Calcium carbonate scale control, effect of material and inhibitors, Water. Sci. Technol. 49 (2004) 153-159.

[3] B. Bansal, M. Steinhagen, Crystallisation fouling in plate heat exchangers, J. Heat. Trans. 115 (1993) 584-591.

[4] J.S. Baker, S.J. Judd, Magnetic amelioration of scale formation, Water Res. 30 (2)(1996) 247–260.

[5] H. Muller-Steinhagen (Ed.), Handbook of Heat Exchanger Fouling-Mitigation andCleaning Technologies, Publico Publications, Germany, 2000.

[6] T.Y. Chen, S.H. Chan, Novel biological inhibitors of fouling and scale formation on heat transfer surfaces through genetic engineering, Nanosc. Microsc. Therm. 4 (2000) 103-108.
[7] X.Y. Wang, B.I. Lee, L. Mann, Dispersion of barium titanate with polyaspartic acid in aqueous media, Colloid. Surface. A. 202 (2002) 71-80.
[8] R. Ketrane, B. Saidani, O. Gil, L. Leleyter, F. Baraud, Efficiency of five scale inhibitors on calcium carbonate precipitation from hard water: effect of temperature and concentration, Desalination 249 (2009) 1397-1404.
[9] L.D. Tijing, H.Y. Kim, D.H. Lee, C.S. Kim, Y.I. Cho, Physical water treatment using RF electric fields for the mitigation of $CaCO_3$ fouling in cooling water, Int. J. Heat. Mass. Tran. 53 (2010) 1426-1437.
[10] F. Alimi, M. Tlili, C. Gabrielli, M. Georges, M. Ben Amor, Effect of a magnetic water treatment on homogene
[11] ous and heterogeneous precipitation of calcium carbonate, Water. Res. 40 (2006) 1941-1950.
[12] M.C. Chang, C.Y. Tai, Effect of the magnetic field on the growth rate of aragonite and the precipitation of $CaCO_3$, Chem. Eng. J. 164 (2010) 1-9.
[13] C.Y. Tai, M.C. Chang, R.J. Shieh, T.G. Chen, Magnetic effects on crystal growth rate of calcite in a constant-composition environment, J. Cryst. Growth. 310 (2008) 3690-3697.
[14] S.H. Lee, Y.I. Cho, Velocity effect on electronic-antifouling technology to mitigate mineral fouling in enhanced-tube heat exchanger, Int. J. Heat. Mass. Tran. 45 (2002) 4163-4174.
[15] X. Xiaokai, Research on the electromagnetic anti-fouling technology for heat transfer enhancement, Appl. Therm. Eng. 28 (2008) 889-894.
[16] A. Shahryari, M. Pakshir, Influence of a modulated electromagnetic field on fouling in a double-pipe heat exchanger, J. Mater. Process. Tech. 203 (2008) 389-395.
[17] C. Piyadasa, H.F. Ridgway, T.R. Yeager, M.B. Stewart, C. Pelekani, S.R. Gray, J.D. Orbell, The application of electromagnetic fields to the control of the scaling and biofouling of reverse osmosis membranes-A review, Desalination 418 (2017) 19-34.
[18] M. Rouina, H.R. Kariminia, S.A. Mousavi, E Shahryari, Effect of electromagnetic field on membrane fouling in reverse osmosis process, Desalination 395 (2016) 41-45.
[19] F. Alimi, M. Tlili, M. Ben Amor, C. Gabrielli, G. Maurin, Influence of magnetic fieldon calcium carbonate precipitation, Desalination 206 (2007) 163–168.
[20] A. Fathi, T. Mohamed, G. Claude, G. Maurin, B.M. Mohamed, Effect of magneticwater treatment on homogeneous and heterogeneous precipitation of calciumcarbonate, Water Res. 40 (2006) 1941–1950.
[21] J.O. Kim, S.P. Choi, H. Yoon, G.T. Kim, Fouling and scaling reduction by pulsed electric field treatment as pre treatment for desalination, Desalin. Water Treat. 43 (2012) 118-123.
[22] L.D. Tijing, D.H. Lee, D.W. Kim, Y.I. Cho, C.S. Kim, Effect of high-frequency electric fields on calcium carbonate scaling, Desalination 279 (2011) 47-53.

[22] Z. Haiquan, Testing and calculate method study on thermal performance and flow pressure drop characteristics of a Plate Heat exchanger, Harbin: Harbin Institute of Technology, 2006.
[23] K.H. Teng, A. Amiri, S.N. Kazi, M.A. Bakar, B.T. Chew, Fouling mitigation on heat exchanger surfaces by EDTA-treated MWCNT-based water nanofluids, J. Taiwan. Inst. Chem. E. 60 (2016) 445-452.
[24] Z. Jiao, A. Satti, X.G. Chen, K. Xiao, J.Y. Sun, X.X. Yan, P. Liang, X.Y. Zhang, X. Huang, Low-voltage electric field applied into MBR for fouling suppression: Performance and mechanisms, CHEM ENG J. 273 (2015) 223-230.

Zhiming Xu received his B.Sc. degree in 1982 from Northeast China Institute of Electric Power, his M.Sc. degree in 1987 from Northeast China Institute of Electric Power and his Ph.D. degree in 1996 from Xi'an Jiaotong University, respectively. He is a Professor of Northeast Electric Power University. His main research interests include fouling and countermeasures of heat-exchanger equipment.